

Simultaneous realization of time and carrier envelope phase synchronization for an ultra-intense few-cycle laser pulse coherent combining system

Guoli Zhang,^{1,2} Xiao Liang,^{1,2,a)} Hao Xue^{1,2,3}, Xinglong Xie,^{1,2,a)} Ping Zhu,^{1,2} Fucui Ding,^{1,2}

Meizhi Sun,^{1,2} Linjun Li,^{1,2} Rashid Ul Haq,^{1,2} Ailin Guo,¹ Xiangbing Zhu,³ Jianqiang Zhu,^{1,2}

¹ *National Laboratory on High Power Laser and Physics, Shanghai Institute of Optics and Fine Mechanics, Chinese Academy of Sciences, Shanghai 201800, People's Republic of China*

² *Center of Materials Science and Optoelectronics Engineering, University of Chinese Academy of Sciences, No. 19(A), Yuquan Road, Shijingshan, Beijing 100049, People's Republic of China*

³ *School of Physics and Electric Information, Anhui Normal University, No. 189 Jiuahuan Road, Wuhu 241002, China*

^{a)} Authors to whom correspondence should be addressed: lx62@siom.ac.cn and xiexl329@siom.ac.cn

Abstract Coherent combining of several low-energy few-cycle beams offers a reliable and feasible approach to producing few-cycle laser pulses with energies exceeding the multi-Joule level. However, time synchronization and carrier-envelope phase difference (ΔCEP) between pulses significantly affect temporal waveform and intensity of the combined pulse, requiring precise measurement and control. Here, we propose a concise optical method based on phase retrieval of spectral interference and quadratic function symmetry axis fitting to simultaneously measure the time synchronization and ΔCEP between few-cycle pulses. The control precision of our coherent beam combining system can achieve a time delay stability

This peer-reviewed article has been accepted for publication but not yet copyedited or typeset, and so may be subject to change during the production process. The article is considered published and may be cited using its DOI.

This is an Open Access article, distributed under the terms of the Creative Commons Attribution licence (<https://creativecommons.org/licenses/by/4.0/>), which permits unrestricted re-use, distribution, and reproduction in any medium, provided the original work is properly cited.

10.1017/hpl.2025.33

within 42 as and Δ CEP measurement precision of 40 mrad, enabling a maximum combining efficiency of 98.5%. This method can effectively improve the performance and stability of coherent beam combining systems for few-cycle lasers, which will facilitate the obtaining of high-quality few-cycle lasers with high energy.

Key words: few-cycle pulse, carrier envelope phase, coherent beam combination, synchronization

I. INTRODUCTION

Few-cycle pulse lasers, as a unique category within the family of ultrashort pulse lasers, have garnered increasing attention due to their distinctive characteristics[1]. For ultra-short lasers tend to reach the peak power at several Petawatts or even Exawatt, few-cycle pulse laser will naturally benefit from the fact that the same energy can be confined to a shorter temporal duration[2, 3]. When the energy of a few-cycle pulse laser exceeds tens of joules, several novel mechanisms in laser-plasma interactions have been unveiled. For instance, proton acceleration driven by an intense few-cycle pulse is particularly advantageous for energy transfer from the laser to the generated ions[4, 5], with a proton cutoff energy greater than GeV being predictable under an instability-free acceleration regime. Similarly, the energy conversion efficiency of laser-to-electron beams has been shown to improve with laser wake field acceleration using few-cycle high-power lasers[6, 7]. Beyond applications in high-energy-density science, the diverse waveforms of few-cycle pulse lasers introduce a new dimension to the study of intense laser field interactions with matter[8]. This capability arises from the fact that the electric field shape of a few-cycle pulse is strongly influenced by the CEP, enabling precise control of atomic-scale

electronic motion [9-11]. The prospect of using a petawatt-class few-cycle laser with a controlled electric field shape in studies of intense laser-matter interactions is both highly intriguing and promising.

However, obtaining Petawatt few-cycle laser pulses remains a significant challenge. Although the peak power of ultrashort pulse laser systems based on chirped-pulse amplification (CPA) or optical parametric chirped-pulse amplification (OPCPA) technology can reach up to 10 PW [12-14], their pulse durations are generally greater than 20 fs. Recently, the post-compression technique was demonstrated to be applicable to a Petawatt class CPA/OPCPA laser by using a thin-film compressor [15]. P. Bleotu et al. reported the successful spectral broadening of a 7 J/21.5 fs laser to a bandwidth compatible with a 15 fs pulse [16], indicating the feasibility of achieving few-cycle pulses in the PW class. Parametric waveform synthesis, by coherently combining laser pulses with different amplified spectra, is another promising technique for obtaining high-power few-cycle or even single-cycle laser pulses with the ability to tailor optical waveforms. A sub-millijoule and sub-cycle (pulse width of 2.8 fs, 0.6 optical cycles at a central wavelength of 1.4 μm) laser pulse was generated by utilizing a parametric waveform synthesis technique [17]. Nonetheless, to generate few-cycle ultrashort pulses with higher power, significant technical challenges remain in the post-compression and parametric waveform synthesis. Here, we propose a direct approach to further increase the peak power of few-cycle lasers, that is, few-cycle pulse coherent combination (FCPCC).

Coherent beam combination can greatly increase laser power far beyond what can be achieved with a single laser and has become a common technique in fiber and diode lasers [18]. While relatively few studies are currently being conducted on FCPCC, two key issues can be foreseen that will seriously deteriorate the combining efficiency of FCPCC. First, time synchronization and

spatial beam pointing are notoriously critical factors in coherent combination, in which time synchronization is more destructive because few-cycle pulses have an extremely narrow pulse duration—typically less than 5 optical cycles. Second, more importantly, coherent combining arises from the interference between the fields of parent few-cycle pulses, and the CEP difference (ΔCEP) between them dramatically deforms the combined laser field. For example, with a CEP shift of π , two pulses will cause destructive interference with the smallest intensity. As an optical pulse propagates through a dispersive material, the CEP evolves due to the difference between phase and group velocities. Consequently, for amplified high-energy few-cycle pulses to be coherently combined, the ΔCEP originates from material thickness variations and refractive index changes caused by inhomogeneities or thermal effects in the amplifier. These factors indicate that minimizing both the time delay and ΔCEP between combined laser pulses is essential for producing stable combined waveforms. Moreover, the deformation of coherent combined pulse waveforms can be very similar when a time delay and ΔCEP appears respectively, making it difficult to distinguish them directly from the retrieved combined light fields [19]. There are methods to control these two parameters individually, such as balanced cross correlation (BOC) [20] for timing jitter and fundamental-to-second-harmonic self-referencing (f-2f) [21] for CEP stabilization. However, in an FCPCC system, implementing f-2f measurements and adjustments for ΔCEP at the final stage of every laser channel would introduce excessive complexity.

In this paper, we present a spectral interference (SI)-based phase difference retrieval method for FCPCC, capable of simultaneously measuring the time delay and ΔCEP with high precision. Our method achieves a time delay measurement resolution of 12 as and controls the standard deviation (STD) of the time delay synchronization within 42 as. The ΔCEP is measured with an accuracy

better than 40 mrad. The experimental implementation demonstrates FCPCC of two laser channels, with real-time feedback control of both the time delay and ΔCEP .

II. The theory of time delay and ΔCEP retrieval

As a linear technique of phase measurement, SI is sensitive and reliable to detect subtle changes between two laser pulses [22]. The theory of SI can be simply described by $I(\omega) = A_1^2 + A_2^2 + 2A_1A_2 \cos(\Phi(\omega))$, in which $\Phi(\omega)$ is their phase difference. The time delay and ΔCEP are the two main phase terms in $\Phi(\omega)$. Consequently, the interferogram of the SI is highly sensitive to these parameters, and variations in $\Phi(\omega)$ can be directly retrieved from the changing fringes of the interferogram. A common method for extracting the time delay from $\Phi(\omega)$ is the Fourier transform algorithm [23]. However, this method is better suited for recovering the time delay longer than the pulse duration, as it avoids overlap of the individual autocorrelation term and interference term when applying the inverse Fourier transform to the spectral interferogram. For FCPCC, the time delay between combined pulses must be minimized to approach zero. In our proposed method, the phase difference is directly retrieved by taking the arccosine of $\cos(\Phi(\omega))$, and the resulting phase difference is subsequently fitted using a quadratic function of ω .

Assuming the central frequency of two pulses is ω_0 , they can be represented in the frequency domain as follows:

$$\begin{aligned} E_1(\omega) &= A_1(\omega)e^{i\varphi_1(\omega)} \\ E_2(\omega) &= A_2(\omega)e^{i(\varphi_2(\omega)+\omega\tau)} \end{aligned} \quad (1)$$

where $A_1(\omega)$ and $A_2(\omega)$ are the amplitude spectra of the pulses, $\varphi_1(\omega)$ and $\varphi_2(\omega)$ are the phase spectra, and τ represents the time delay between the two pulses. For chirped pulses, the phase spectra can typically be expanded using a quadratic polynomial:

$$\begin{aligned}\varphi_1(\omega) &= \varphi_1(\omega_0) + GD_1(\omega - \omega_0) + \frac{1}{2}GDD_1(\omega - \omega_0)^2 + o(\omega^3) \\ \varphi_2(\omega) &= \varphi_2(\omega_0) + GD_2(\omega - \omega_0) + \frac{1}{2}GDD_2(\omega - \omega_0)^2 + o(\omega^3)\end{aligned}\quad (2)$$

Here, $\varphi_1(\omega_0)$ and $\varphi_2(\omega_0)$ denote the carrier phase shifts, GD_1 and GD_2 represent the group delays (GD), and GDD_1 and GDD_2 denote the group delay dispersion (GDD). $o(\omega^3)$ is referred to as high-order dispersion, which has a relatively minor impact on the calculation compared to GDD. Therefore, it can be neglected during the formula derivation process. However, achieving higher measurement accuracy requires precise correction of the bias introduced by third-order dispersion (TOD). For further details, please refer to the supplementary materials. Then we can get

$$\Phi(\omega) = \frac{1}{2}\Delta GDD \cdot \omega^2 + (\Delta GD - \tau - \Delta GDD \cdot \omega_0)\omega + \frac{1}{2}\Delta GDD \cdot \omega_0^2 + \Delta\varphi_0 - \Delta GD \cdot \omega_0 \quad (3)$$

where $\Delta\varphi_0 = \varphi_1(\omega_0) - \varphi_2(\omega_0)$, $\Delta GD = GD_1 - GD_2$, $\Delta GDD = GDD_1 - GDD_2$. The above expression shows that when $\Delta GDD \neq 0$, $\Phi(\omega)$ is a quadratic function of ω . Since ΔGD represents the group delay, combining ΔGD with τ yields the actual time delay

$$t_d = \Delta GD - \tau \quad (4)$$

According to the basic properties of a quadratic function, there is a symmetry axis

$$\omega_s = \frac{\Delta GDD \cdot \omega_0 - t_d}{\Delta GDD} \quad (5)$$

Thus, the actual time delay between the two pulses can be solved from the symmetry axis as:

$$t_d = \Delta GDD \cdot (\omega_0 - \omega_s) \quad (6)$$

It is obvious that ω_s is linearly related to t_d at the symmetry axis, and $t_d = 0$ when $\omega_s = \omega_0$. ΔGDD is obtained directly from the coefficient of the quadratic term of the fitted phase expression. From Eq. (3), when $t_d = 0$, we have:

$$\Phi(\omega_0) = \Delta\varphi_0 - \Delta GD \cdot \omega_0 \quad (7)$$

Since the CEP refers to the phase difference between the carrier and the envelope

$$\begin{aligned}\varphi_{1,CEP} &= \varphi_1(\omega_0) - \omega_0 \cdot GD_1 \\ \varphi_{2,CEP} &= \varphi_2(\omega_0) - \omega_0 \cdot GD_2\end{aligned}\quad (8)$$

Thus, the ΔCEP between the two pulses

$$\Delta CEP = \varphi_{1,CEP} - \varphi_{2,CEP} = \Phi(\omega_0)\quad (9)$$

The above derivation demonstrates that for two pulses with group delay dispersion differences, the time delay and ΔCEP between the two pulses can be determined by analyzing the parabolic characteristics of the spectral interference phase. By further adjusting the time delay to zero, the phase value of the central frequency of the pulse corresponds to the ΔCEP between the two pulses.

Consequently, both the time delay and ΔCEP can be simultaneously resolved, enabling the realization of time and CEP synchronization. Indeed, ΔGDD is necessary and the key point in this method because the function of $\Phi(\omega)$ is quadratic only when there is ΔGDD between two laser beams. In an FCPCC system, ΔGDD naturally arises because the pulse duration must be stretched by dispersion components and pass through the OPCPA to achieve energy amplification. This condition also indicates an advantage of our method in that the time delay and ΔCEP can be measured and controlled before dispersion compensation.

III. Experiment to the FCPCC of two few-cycle laser beams

An FCPCC system consisting of two few-cycle pulses was demonstrated to verify the proposed measurement method for the time delay and ΔCEP . As shown in Fig. 1, the laser seed was a commercial Ti:sapphire mode-locked femtosecond laser, delivering 10 fs pulses with 20 nJ of energy at a central wavelength of 800 nm. This pulse duration corresponds to approximately four optical cycles. The laser pulse was split into two channels by a 50/50 beam splitter. The

transmission channel (designated as channel 1) from the splitter had an additional dispersion and an altered CEP. The CEP of channel 1 was further actively controlled by passing through a wedge pair, where one wedge was mounted on a moving stage driven by a DC motor to precisely adjust the wedge thickness. The wedge pair, made of fused silica, had a wedge angle of 1 mrad. In addition to introducing a difference in CEP, the movement of the wedge also introduced changes in the time delay between channel 1 and channel 2. In our setup, the closed-loop control precision of the piezo-driven delay line (PZD) is 0.6 nm. Specifically, we used the NFL5DP20S/M model from Thorlabs, paired with the KPC101 controller, both of which are well-suited for high-precision applications. The coherent combination of the two laser channels, implemented in a tiled-aperture configuration, was achieved using an off-axis parabolic (OAP) mirror with a focal length of 381 mm. Before combination, the dispersion of the two laser pulses was compensated by chirped mirrors. As shown in Fig. 2, the pulse durations of the two channels were measured by a FROG system to be 10.4 fs and 10.9 fs, respectively. These results confirm that the two pulses used for coherent combining were indeed few-cycle pulses, corresponding to approximately 4 optical cycles at a wavelength of 800 nm. To a large extent, in terms of time delay, dispersion and CEP, our experimental setup can simulate the actual situation of coherent combination of two high energy few-cycle pulses. Moreover, in the high energy few-cycle system, the grating-based compressor is typically required for the dispersion compensation as it can offer large amount of GDD. However, the grating compressor also introduces fluctuations in the CEP. To obtain Fourier transform limited pulses, chirped mirror pairs are necessary to provide accurate dispersion compensation. Our Δ CEP measurement can be implemented between these two stages, allowing control over the CEP fluctuations introduced by the grating compressor.

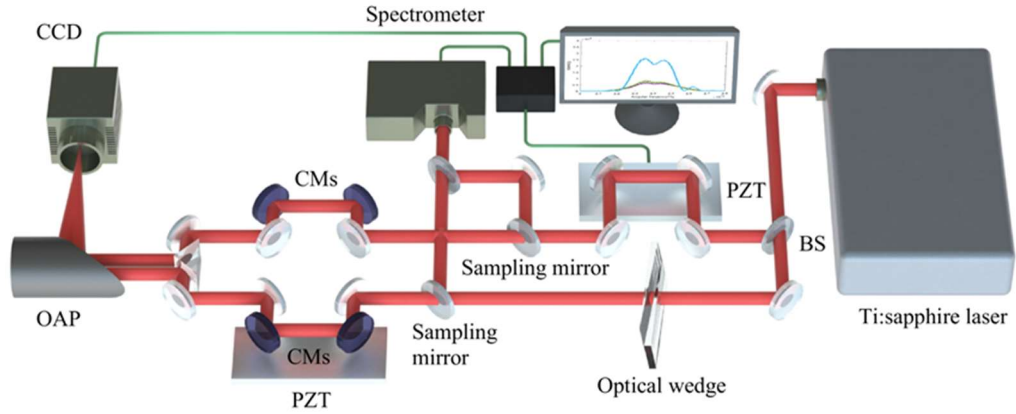


Fig. 1. Experimental setup of the FCPCC with a SI system for the measurement of time synchronization and Δ CEP. A commercial Ti:sapphire mode-locked femtosecond laser provided 10 fs pulses with 20 nJ of energy at a central wavelength of 800 nm. The laser pulse was split by a 50/50 beam splitter (BS), where laser channel 1 passed through a wedge pair for active CEP control, while laser channel 2 passed only through a time delay controller mounted on a PZD stage. Both laser channels were sampled for phase difference measurements based on spectral interference. The remaining portions of the lasers were coherently combined in a tiled-aperture configuration, and the far-field interferogram was captured using a CCD camera. Before combination, the two channels were passed through chirped mirrors (CMs) for dispersion compensation.

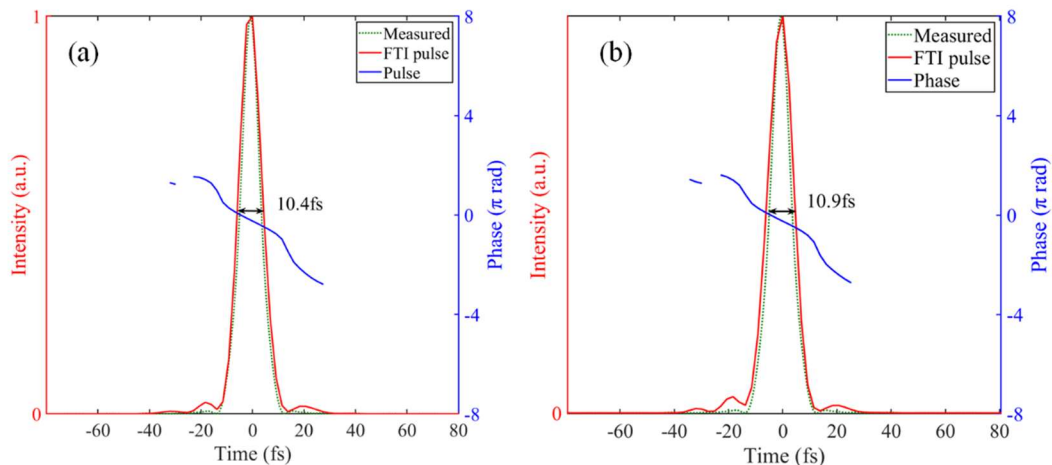


Fig. 2. Measured pulse durations of the two laser channels. (a) The pulse duration of channel 1 is 10.4 fs, (b) the pulse duration of channel 2 is 10.9 fs. Both pulse durations correspond to approximately 4 optical cycles at a central wavelength of 800 nm. The Fourier transform limits according to the spectrum are both 9.3 fs for both channels, as shown by the dotted lines.

The SI was implemented using a Mach–Zehnder interferometer, as shown in Fig. 1. The two interference arms were sampled from laser channels 1 and 2 and recombined in a collinear geometry through a beam splitter. The interferogram produced by the SI was collected by a spectrometer (Ocean Optics, HR4000+). The data were analyzed using a quadratic function fitting method to extract the time delay and ΔCEP , which was subsequently feedback to the PZD and DC motor for active control of these two parameters. Fig. 3 presents the spectral interferogram and the retrieved phase difference of two laser pulses at different time delays. Although the retrieved phase difference (orange curve) is not phase unwrapped, a quadratic curve (red curve) can still be fitted in all cases. The symmetry axis ω_s of the fitted quadratic curve (blue dotted line) determines the angular frequency difference ($\Delta\omega$) between ω_s and ω_0 . Omitting the phase unwrapping step reduces the computation time for solving the time delay. Using Eq. (6), the time delays shown in Fig. 3 were determined to be 1.31 fs, 4.85 fs, and 24.10 fs, respectively. As ω_s approaches ω_0 , the time delay decreases. When $\Delta\omega$ is less than the fitting resolution of our SI method, the time delay is considered to be zero, indicating that the two laser pulses are time-synchronized. The spectral resolution of the spectrometer used in our setup is 0.2 nm. Our measurement method achieves a temporal resolution of 12 as, with further analysis provided in the Discussion section and Supplementary Material.

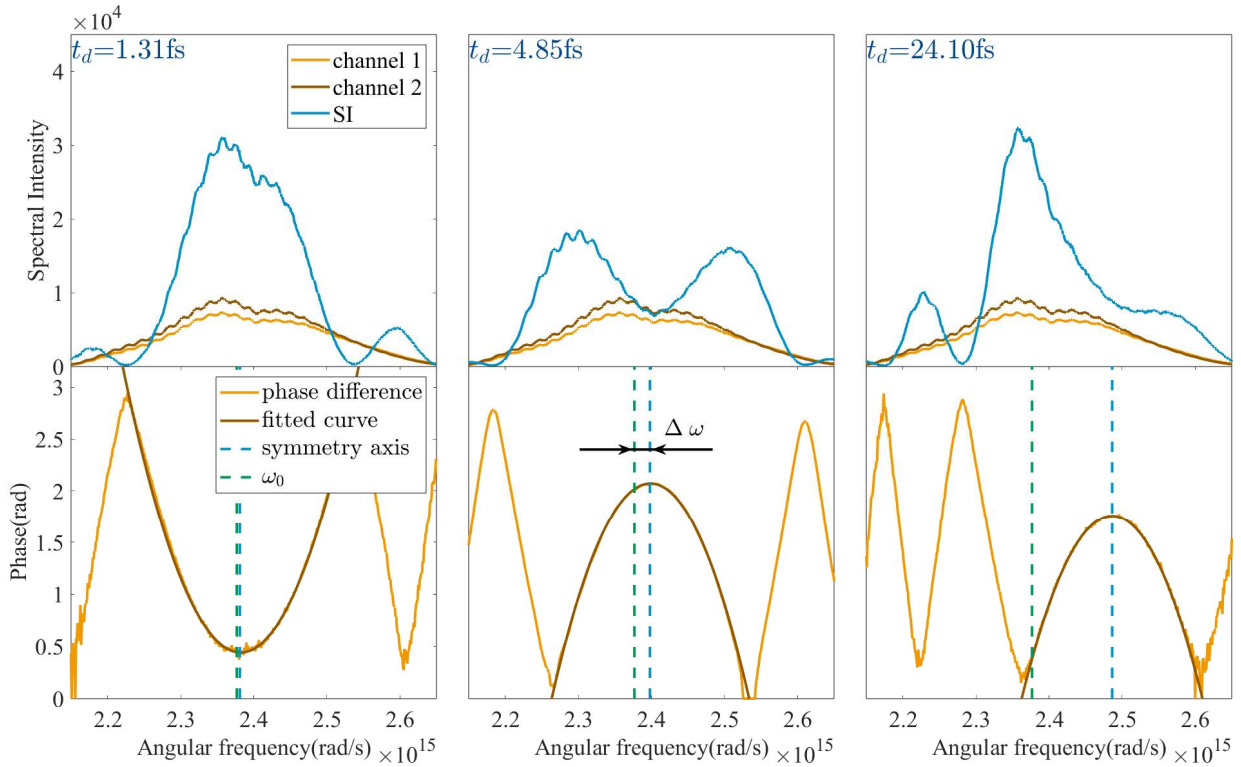


Fig. 3. Spectral interferogram and retrieved phase difference of two laser pulses at different time delays. Each retrieved phase difference (orange curve) from the spectral interferogram is fitted with a quadratic curve (red curve). The symmetry axis (blue dotted line) determines the angular frequency difference $\Delta\omega = \omega_0 - \omega_s$, from which the time delay (t_d) can be calculated.

Subsequently, ΔCEP can be determined using Eq. (2). When the time delay t_d is equal to zero, the retrieved phase difference $\Phi(\omega_s)$ corresponds to ΔCEP . Fig. 4 presents the spectral interferogram for this condition, where all the symmetric axis of the quadratic fitted curves align with the central frequency ω_0 . ΔCEP values of 0.027 rad, 1.534 rad and 2.950 rad were measured for three different interferograms, as shown in Fig. 4. Without active feedback control, environmental disturbances—such as mechanical vibrations and air currents—caused significant time delay drifts, as shown in Fig. 5(a). These drifts led to a loss of temporal stability, with large

fluctuations observed over time. Engaging the active feedback system effectively suppressed low-frequency noise components, as shown by the reduced time delay fluctuations in the latter portion of Fig. 5(a) and the corresponding frequency spectrum in Fig. 5(b).

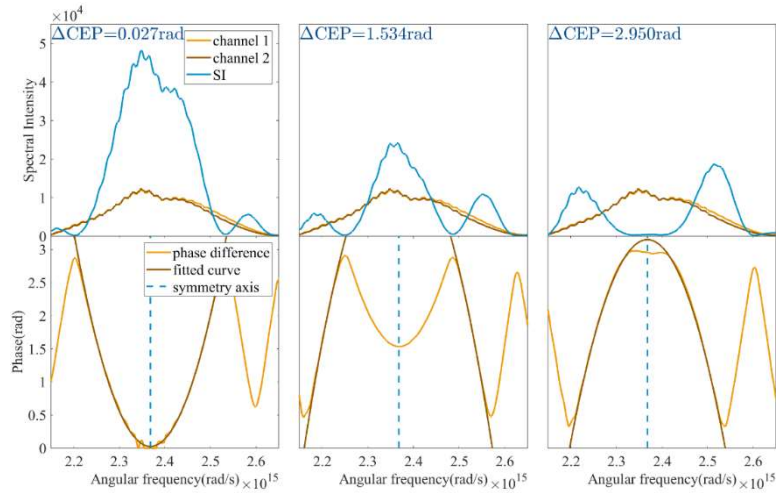


Fig. 4. Spectral interferogram and retrieved phase difference of two synchronized laser pulses at different ΔCEP values. When the symmetry axis ω_s of the quadratic curve aligns with ω_0 , t_d is determined to be zero; then, the retrieved phase difference at the symmetry axis corresponds directly to ΔCEP .

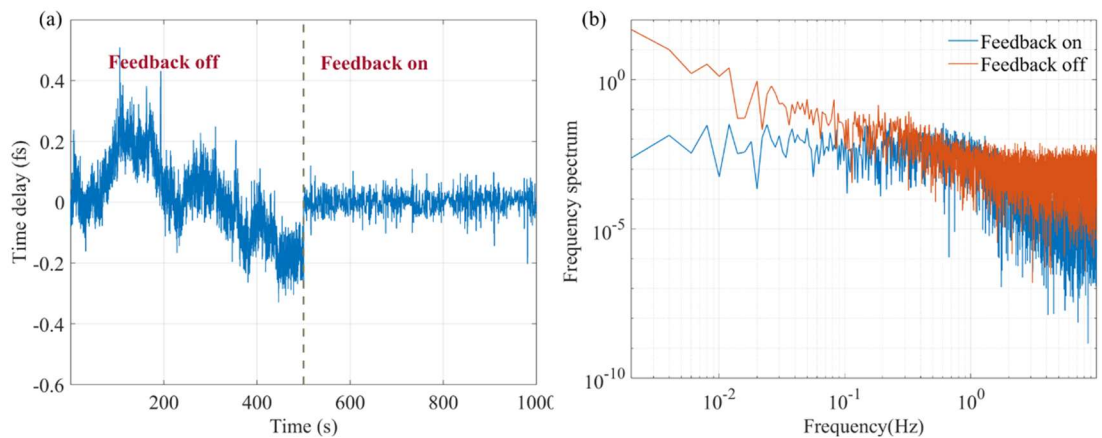


Fig. 5 Time Delay Stability (a) and Jitter Power Spectrum (b) with Feedback on and off

To further validate our ability to precisely measure and control ΔCEP , the wedge thickness was adjusted to span ΔCEP across a range of π in our experiment, with the measurement results depicted as the orange signal in Fig. 6. The optical wedge was adjusted by 1 mm every few minutes while maintaining time synchronization (blue signal). Each step of wedge adjustment induced a measured variation in ΔCEP of approximately 0.105 rad. Starting at -1.72 rad, ΔCEP reached 2.28 rad after 38 adjustments. Both the blue and orange signals exhibit fine spikes, representing instantaneous changes in the time delay and ΔCEP detected during incremental adjustments of the wedge thickness by the DC motor. Abrupt changes in the time delay were immediately corrected by the feedback system. During prolonged feedback stabilization, the STD of the time delay was effectively controlled to within 42 as.

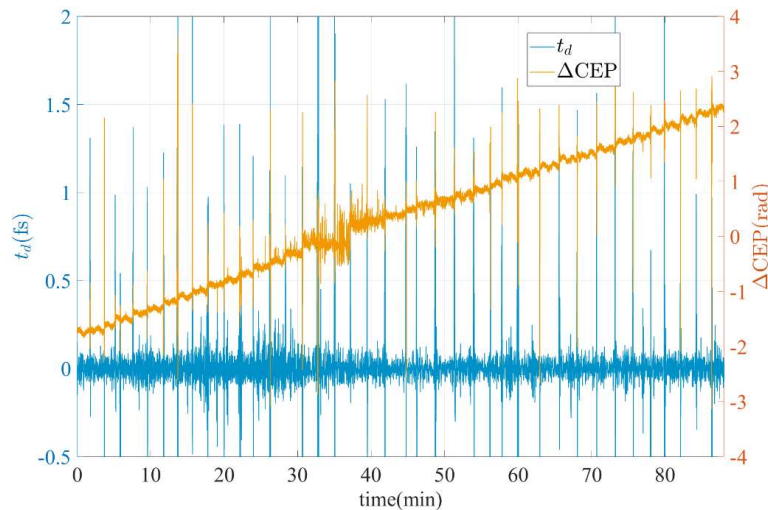


Fig. 6. Measurement results of continuously varying ΔCEPs within a range larger than π while maintaining time synchronization. The blue signal represents the measured time delay, and the orange signal represents the measured ΔCEP . The spikes observed in both signals correspond to instantaneous changes in the time delay and ΔCEP , detected during incremental adjustments of the wedge thickness.

With the control of ΔCEP while keeping time synchronized, we observed the FCPCC using a CCD camera. Spatial interference fringes formed in the far-field due to the tiled-aperture configuration. Notably, this configuration of FCPCC is highly efficient, as it avoids the energy loss and potential damage to the combining mirrors, making it suitable for high-energy system at hundred milli-joule or joule level. Laboratories aiming to achieve Exawatt-class lasers through the coherent combination of Petawatt lasers predominantly employ tiled-aperture configuration [24, 25]. Fig. 7(a) shows the central cross-section of the far-field interference fringes for varying ΔCEP values. As ΔCEP is varied, the strongest fringe gradually shifts, demonstrating the linear movement of interference fringes. This result confirms that the measurement and regulation of ΔCEP were effectively achieved based on time synchronization through SI. To further characterize the FCPCC performance, we calculated the combining efficiency for each ΔCEP value and compared it with numerical simulations based on angular spectrum method. The combining efficiency is defined as the ratio of the focused peak intensity of the combined beam to the maximum achievable value under perfectly coherent conditions [26]. As shown in Fig. 7(b), the experimental combining efficiency (solid line) aligns very well with the simulated efficiency (dashed line). The highest combining efficiency, approximately 98.5%, is reached for $\Delta\text{CEP} = 0$ (blue dot c), while the efficiency drops to 85.6% when $\Delta\text{CEP} = \pi$ (blue dot e). The highest combining efficiency doesn't reach 100% because of a measured ΔGDD of 5 fs^2 between the two combined pulses, which also accounts for the slight differences in pulse durations shown in Fig. 2. Notably, the relative ΔCEP measured in the SI setup shown in Fig. 1 differs from the actual ΔCEP in the far-field combined beam. However, the relative phase difference between these two positions remains constant, and we initially calibrated the phase difference and time delay using

the same SI method. Detailed information on calibration can be found in the Supplementary Material. The relative phase difference of ΔCEP in our experiment was determined to be 1.5 rad. Additionally, minor modifications to the experimental setup in Fig. 1 enabled beam combining in a filled-aperture configuration. A beamsplitter sampled the combined pulse entering the spectrometer and directed a portion to a CCD camera for focal spot intensity monitoring. Employing the same experimental procedure as in Fig. 7(a), we observed the combined beam profile behavior depicted in Fig. 7(f). In this configuration, as the two pulses co-propagate axially, no fringe movement was observed. Instead, significant intensity modulation occurred in the combined focal spot. The ΔGDD between the combined pulses, measured to be approximately 220 fs². This relatively high ΔGDD produced variations in combining efficiency ranging from 20% to 80%, in strong agreement with our simulations, as illustrated in Fig. 7(g). These experimental results reveal that in the far-field coherent combining, a noncollinear configuration is more robust against ΔCEP variations compared to a collinear configuration, which results in destructive interference when $\Delta\text{CEP} = \pi$. However, ΔCEP can still cause approximately 15% efficiency decline. The experimental results from Fig. 6 and Fig. 7 demonstrate the precise ΔCEP control in both configurations, while simultaneously ensuring accurate time synchronization.

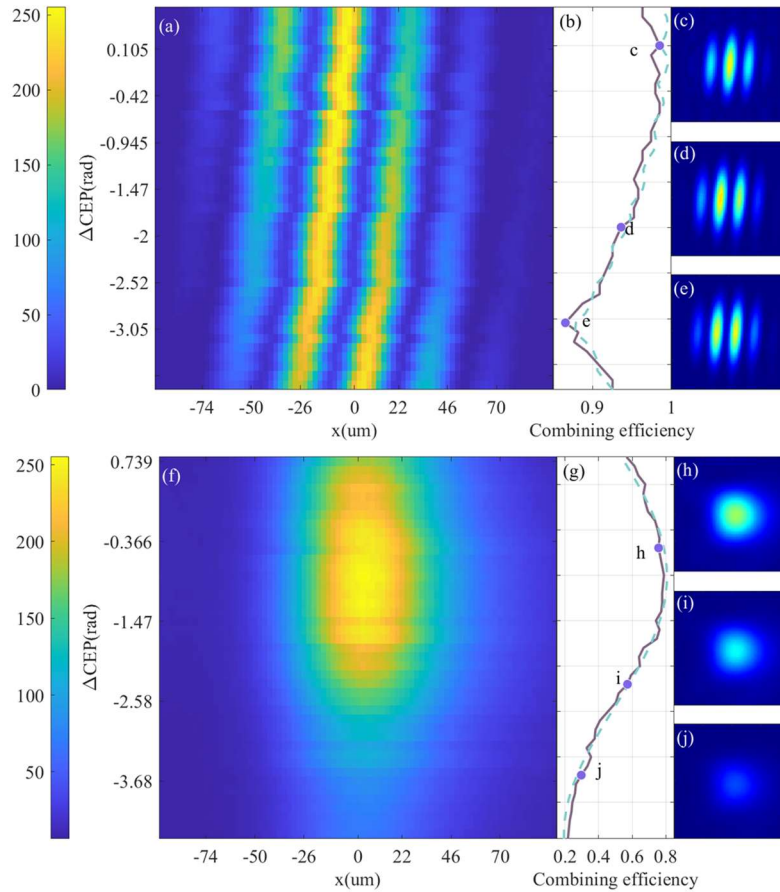


Fig. 7. Far-field interference fringes and efficiency obtained of the FCPCC under different ΔCEP values in the tiled (a) and filled-aperture (f) configurations. The strongest interference fringe in Fig. 7(a) gradually shifts with increasing ΔCEP , and the highest combining efficiency (98.5%) is reached only when $\Delta\text{CEP} = 0$. For the filled-aperture configuration in Fig. 7(f), there is no interference fringe, and the maximum beam combining intensity is also reached when $\Delta\text{CEP}=0$. The solid line in Fig. 7(b), (g) show the experimentally obtained combining efficiency, while the dashed line corresponds to the simulation results based on the experimental parameters. Additionally, Fig. 7(c–e) and Fig. 7(h–j) depict the spatial interference patterns observed at three distinct ΔCEP values identified on the efficiency curves in Fig. 7(b) and Fig. 7(g), respectively. These patterns further illustrate the dependence of the combining performance on ΔCEP for each configuration.

IV. Discussion

The accuracy of the Δ CEP measurements was evaluated by comparison with the theoretical values derived from the experimental setup. The dotted blue line in Fig. 8 represents the theoretical Δ CEP variation induced by translating the optical wedges. In the experiment, when the wedge is displaced by 1 mm, the thickness changes by 1 μm due to its wedge angle of 1 mrad. Based on the data in Fig. 6, the mean value of the measured Δ CEP at each step is fitted to produce the green line in Fig. 8, and the measurement STD is shown as a gray line. The Δ CEP measurement shows good agreement with the ideal linear relationship dictated by the optical wedge thickness variation, as evident in Fig. 8. The fused silica wedge used in the experiment exhibits minimal surface profile error, enabling the thickness variation to be treated as ideal and linear, resulting in a corresponding Δ CEP variation that is also linear. Surface profile measurements of the wedge, detailed in the Supplementary Materials, confirm that its contribution to the overall error is negligible. For a laser pulse with a central wavelength of 800 nm, a thickness variation of 1 μm corresponds to a Δ CEP change of approximately 107 mrad.

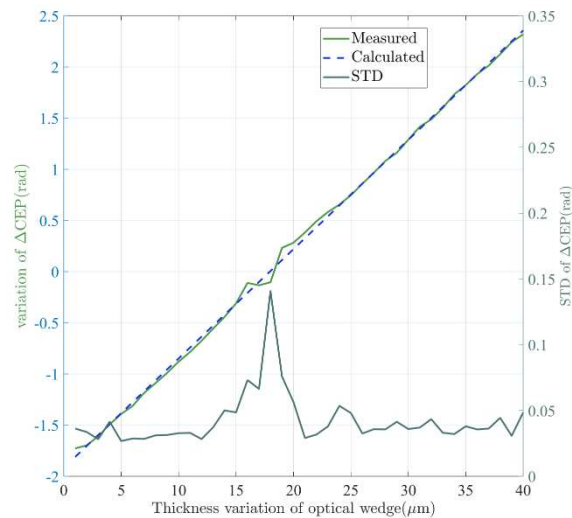


Fig. 8. Comparison of the variation in ΔCEP between the measured results and theoretical values. The dotted blue line represents the theoretical ΔCEP variation induced by wedge translation, while the green line is fitted to the mean measured ΔCEP values at each step of Fig. 5. The gray line represents the STD of each measurement, in which the mean STD is 40 mrad.

Our measurement results show a ΔCEP variation of 105 mrad/ μm , which aligns closely with the intrinsic material parameter of 107 mrad/ μm with an error below 2%. The mean STD of the ΔCEP measurements is about 40 mrad at points farther from $\Delta\text{CEP} = 0$ rad, demonstrating the good accuracy and stability of our method in these regions. However, the STD increases significantly near $\Delta\text{CEP} = 0$ rad, reaching approximately 140 mrad, due to higher sensitivity to time delay jitter in this region. When the repetition rate of the laser pulse far exceeds the spectrometer's acquisition frequency, the spectral interference signal represents the cumulative result of multiple interferences. Consequently, the calculated spectral phase difference reflects an averaged value over the acquisition cycle, which prevents complete constructive or destructive interference, as shown by the solid line in Fig. 9. To examine this, simulations incorporating time delays and third-order dispersion were compared with experimental data. As shown in the results, the spectral phase difference between the two pulses was distorted at 0 and π . By adding random time-delay jitter (0.15 fs) to simulate the spectrometer's integration process, the noisy simulated phase φ_{noise} , closely matched the experimental results φ_{exp} , compared to the phase φ_{ideal} under ideal conditions, as illustrated by the chain line in Fig. 9, confirming that the incomplete interference originates from spectrometer averaging. As shown in Fig. 4, under the same experimental conditions, when $\Delta\text{CEP} = 2.95$ rad, more pronounced phase distortion is observed near the central frequency. To further reduce measurement deviation, achieving shorter exposure times and enhanced mechanical stability is highly necessary.

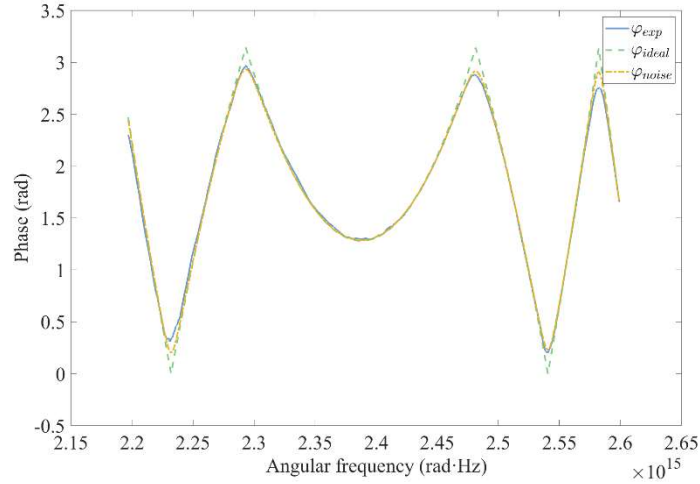


Fig. 9. Experimental spectral phase difference (solid line) and noisy simulated phase (dashed line) considering the impact of the time jitter of multiple pulses

In the experiment, we calculate the time delay by fitting a quadratic function to the spectral phase difference to obtain the symmetry axis ω_s , which is subsequently solved according to Eq. (6). Given the exceptional stability of ΔGDD , the resolution of the fit to the symmetry axis directly determines the resolution of the time delay. The spectrometer used in the setup has a pixel resolution of 0.2 nm. To balance computational accuracy and efficiency, 10 points are selected from the phase data for each fit, and the symmetry axis resolution is determined to be 55 GHz using the error propagation method. Furthermore, the corresponding temporal delay resolution can be calculated using Eq. (6), yielding a value of approximately 12 as. Detailed calculations are provided in the supplementary materials.

By substituting Eq. (4), Eq. (6), and Eq. (8) into Eq. (7) from the manuscript, we obtain the following formula when $\omega = \omega_0$,

$$\Delta\text{CEP} = \Phi(\omega_0) - \omega_0 \cdot t_d \quad (10)$$

This is the formula we used to obtain the ΔCEP values in our experiment. Under the current experimental conditions, when the optical wedge remains stationary, ΔCEP is relatively stable.

Therefore, variations in ΔCEP are primarily caused by changes in the phase at the central frequency and the time delay. Using the error propagation formula:

$$\sigma(\Delta\text{CEP}) = \sigma(\Phi(\omega_0)) + \omega_0 \cdot \sigma(t) \quad (11)$$

In our current experiment, only a single spectrum was collected before the interference of the two pulses, making it necessary to consider the impact of light source power stability on the measurements. Since $\Phi(\omega_0) = \cos^{-1}\left(\frac{I - I_1 - I_2}{2\sqrt{I_1 I_2}}\right)$, the error propagation formula can be expressed as:

$$\sigma(\Phi(\omega_0)) = \frac{\sigma_I}{2\sqrt{I_1 I_2} \sqrt{1 - \cos^2 \Phi(\omega_0)}} \quad (12)$$

From the above equation, it can be observed that $\Phi(\omega_0)$ exhibits greater uncertainty at 0 or π . This, in turn, explains why a measurement deviation of 140 mrad was observed when $\Delta\text{CEP} = 0$. To achieve the optimal resolution of the system, measurement points near $\cos(\Phi(\omega_0)) = 0$ should be selected, as the error amplification factor is minimized and the system resolution is maximized at this condition. At this point, $\Phi(\omega_0) = \pi/2$. The spectral integration time was 10 ms, corresponding to a spectral energy fluctuation $\sigma_I = 0.5\%$, which is relatively small and stable. A 0.5% fluctuation in light intensity will induce an approximately linear variation in $\sigma(\Phi(\omega_0))$. Then, we calculated $\sigma(\Phi(\omega_0)) = 5$ mrad. Given that $\omega_0 \cdot \sigma(t_d) = 28$ mrad, the measurement resolution of ΔCEP is determined to be 33 mrad. The current measurement precision is already approaching the resolution limit of the system under the present experimental conditions. By increasing the number of sampling points and real-time monitoring of light source fluctuations, it is possible to further improve the measurement resolution and system stability. However, this improvement comes at the cost of significantly longer computation times and higher operational expenses. Therefore, in practical applications, a balance must be struck between feedback speed and precision. We cannot further control these errors in our experiments because the speed of our feedback loop is much

slower than the frequency of the errors; in other words, the upper bandwidth limit of our feedback loop is 100 Hz, which is mainly restricted both by the response time of the PZD and the acquisition frequency of the spectrum meter.

V. Conclusion

In conclusion, we proposed a method for generating high-energy few-cycle laser pulses through the coherent combination of low-energy pulses, using a concise optical approach based on spectral interference to simultaneously synchronize time delay and CEP. Without involving nonlinear optical processes, this method has quite a low requirement for laser energy, which makes it possible to integrate these measurements on a chip-based spectrometer [27, 28]. In addition to a few-cycle laser, the time delay measurement and control can be extended to femtosecond lasers and picosecond lasers. Notably, this method remains robust and scalable when applied to high-energy few-cycle pulse systems. Its ability to perform single-shot spectral sampling for each pulse eliminates measurement errors caused by energy fluctuations, which is critical for the coherent combination of amplified lasers with lower repetition rates. We prospect that in the next step of our work, this method will be exploited in the coherent combination of several amplified few-cycle lasers with tens millijoule energy, which can further push the energy of few-cycle laser pulse to the Joule level.

Acknowledgement

This work is supported by the Key projects of intergovernmental international scientific and technological innovation cooperation (2021YFE0116700), National Natural Science Foundation of China (NSFC) (12204500, 12074399), Shanghai Sailing Program (22YF1455300), Chinese Academy of Sciences (XDA25020105, XDA25020103, XDA25020101).

References

1. J. A. Wheeler, G. Mourou, and T. Tajima, "Science of High Energy, Single-Cycled Lasers," *Reviews of Accelerator Science and Technology* 10, 227-244 (2019). DOI: <https://doi.org/10.1142/s1793626819300123>
2. D. E. Rivas, A. Borot, D. E. Cardenas, G. Marcus, X. Gu, D. Herrmann, J. Xu, J. Tan, D. Kormin, G. Ma, W. Dallari, G. D. Tsakiris, I. B. Foldes, S. W. Chou, M. Weidman, B. Bergues, T. Wittmann, H. Schroder, P. Tzallas, D. Charalambidis, O. Razskazovskaya, V. Pervak, F. Krausz, and L. Veisz, "Next Generation Driver for Attosecond and Laser-plasma Physics," *SCIENTIFIC REPORTS* 7(2017). DOI: <https://doi.org/10.1038/s41598-017-05082-w>
3. Z. Li, Y. Kato, and J. Kawanaka, "Simulating an ultra-broadband concept for Exawatt-class lasers," *Scientific Reports* 11, 151 (2021). DOI: <https://doi.org/10.1038/s41598-020-80435-6>
4. M. L. Zhou, X. Q. Yan, G. Mourou, J. A. Wheeler, J. H. Bin, J. Schreiber, and T. Tajima, "Proton acceleration by single-cycle laser pulses offers a novel monoenergetic and stable operating regime," *Physics of Plasmas* 23(2016). DOI: <https://doi.org/10.1063/1.4947544>
5. X. Wu, Z. Gong, Y. Shou, Y. Tang, J. Yu, G. Mourou, and X. Yan, "Efficiency enhancement of ion acceleration from thin target irradiated by multi-PW few-cycle laser pulses," *Physics of Plasmas* 28(2021). DOI: <https://doi.org/10.1063/5.0029171>
6. D. Papp, Z. LécZ, C. Kamperidis, and N. A. Hafz, "Highly efficient few-cycle laser wakefield electron accelerator," *Plasma Physics and Controlled Fusion* 63, 065019 (2021). DOI: <https://doi.org/10.1088/1361-6587/abf80d>
7. Z. LécZ, A. Andreev, D. Papp, C. Kamperidis, and N. A. Hafz, "Three-stage laser wakefield accelerator scheme for sub-Joule few-cycle laser pulses," *Plasma Physics and Controlled Fusion* 65, 105001 (2023). DOI: <https://doi.org/10.1088/1361-6587/aceeb2>
8. E. Ridente, M. Mamaikin, N. Altwajry, D. Zimin, M. F. Kling, V. Pervak, M. Weidman, F. Krausz, and N. Karpowicz, "Electro-optic characterization of synthesized infrared-visible light fields," *Nature communications* 13, 1111 (2022). DOI: <https://doi.org/10.1038/s41467-022-28699-6>

9. T. T. Luu, M. Garg, S. Y. Kruchinin, A. Moulet, M. T. Hassan, and E. Goulielmakis, "Extreme ultraviolet high-harmonic spectroscopy of solids," *Nature* 521, 498-502 (2015). DOI: <https://doi.org/10.1038/nature14456>
10. S.-W. Huang, G. Cirmi, J. Moses, K.-H. Hong, S. Bhardwaj, J. R. Birge, L.-J. Chen, E. Li, B. J. Eggleton, and G. Cerullo, "High-energy pulse synthesis with sub-cycle waveform control for strong-field physics," *Nature photonics* 5, 475-479 (2011). DOI: <https://doi.org/10.1038/nphoton.2011.140>
11. E. Goulielmakis, M. Schultze, M. Hofstetter, V. S. Yakovlev, J. Gagnon, M. Uiberacker, A. L. Aquila, E. Gullikson, D. T. Attwood, and R. Kienberger, "Single-cycle nonlinear optics," *Science* 320, 1614-1617 (2008). DOI: <https://doi.org/10.5772/37416>
12. I. B. Mukhin, A. A. Soloviev, E. A. Perevezentsev, A. Shaykin, V. N. Ginzburg, I. V. e. Kuzmin, M. A. Mart'yanov, I. y. A. Shaikin, A. A. Kuzmin, and S. Y. Mironov, "Design of the front-end system for a subexawatt laser of the XCELS facility," *Quantum Electronics* 51, 759 (2021). DOI: <https://doi.org/10.1070/QEL17620>
13. J. Bromage, S.-W. Bahk, I. Begishev, C. Dorrer, M. Guardalben, B. Hoffman, J. Oliver, R. Roides, E. Schiesser, and M. Shoup Iii, "Technology development for ultraintense all-OPCPA systems," *High Power Laser Science and Engineering* 7, e4 (2019). DOI: <https://doi.org/10.1017/hpl.2018.64>
14. C. Radier, O. Chalus, M. Charbonneau, S. Thambirajah, G. Deschamps, S. David, J. Barbe, E. Etter, G. Matras, S. Ricaud, V. Leroux, C. Richard, F. Lureau, A. Baleanu, R. Banici, A. Gradinariu, C. Caldararu, C. Capiteanu, A. Naziru, B. Diaconescu, V. Iancu, R. Dabu, D. Ursescu, I. Dancus, C. A. Ur, K. A. Tanaka, and N. V. Zamfir, "10 PW peak power femtosecond laser pulses at ELI-NP," *High Power Laser Science and Engineering* 10, e21 (2022). DOI: <https://doi.org/10.1017/hpl.2022.11>
15. S. Y. Mironov, S. Fourmaux, P. Lassonde, V. Ginzburg, S. Payeur, J.-C. Kieffer, E. Khazanov, and G. Mourou, "Thin plate compression of a sub-petawatt Ti: Sa laser pulses," *Applied Physics Letters* 116(2020). DOI: <https://doi.org/10.1063/5.0008544>
16. P.-G. Bleotu, J. Wheeler, S. Y. Mironov, V. Ginzburg, M. Masruri, A. Naziru, R. Secareanu, D. Ursescu, F. Perez, and J. De Sousa, "Post-compression of high-energy, sub-picosecond laser pulses," *High Power Laser Science and Engineering* 11, e30 (2023). DOI: <https://doi.org/10.1364/HPSLP.1989.M3>
17. G. M. Rossi, R. E. Mainz, Y. D. Yang, F. Scheiba, M. A. Silva-Toledo, S. H. Chia, P. D. Keathley, S. B. Fang, O. D. Muecke, C. Manzoni, G. Cerullo, G. Cirmi, and F. X. Kaertner, "Sub-cycle millijoule-level parametric waveform synthesizer for attosecond science," *Nature Photonics* 14, 629-+ (2020). DOI: <https://doi.org/10.1038/s41566-020-0659-0>
18. M. Veinhard, S. Bellanger, L. Daniault, I. Fsaifes, J. Bourderionnet, C. Larat, E. Lallier, A. Brignon, and J.-C. Chanteloup, "Orbital angular momentum beams generation from 61 channels coherent beam combining femtosecond digital laser," *Optics Letters* 46, 25-28 (2020). DOI: <https://doi.org/10.1364/OL.405975>
19. C. Manzoni, O. D. Mucke, G. Cirmi, S. B. Fang, J. Moses, S. W. Huang, K. H. Hong, G. Cerullo, and F. X. Kartner, "Coherent pulse synthesis: towards sub-cycle optical waveforms," *Laser & Photonics Reviews* 9, 129-171 (2015). DOI: <https://doi.org/10.1002/lpor.201400181>

20. A. J. Benedick, J. G. Fujimoto, and F. X. Kärtner, "Optical flywheels with attosecond jitter," *Nature Photonics* 6, 97-100 (2012). DOI: <https://doi.org/10.1038/nphoton.2011.326>
21. M. Schultze, A. Wirth, I. Grguras, M. Uiberacker, T. Uphues, A. J. Verhoef, J. Gagnon, M. Hofstetter, U. Kleineberg, and E. Goulielmakis, "State-of-the-art attosecond metrology," *Journal of Electron Spectroscopy and Related Phenomena* 184, 68-77 (2011). DOI: <https://doi.org/10.1063/1.1470288>
22. L. Lepetit, G. Chériaux, and M. Joffre, "Linear techniques of phase measurement by femtosecond spectral interferometry for applications in spectroscopy," *J. Opt. Soc. Am. B* 12, 2467-2474 (1995). DOI: <https://doi.org/10.1364/JOSAB.12.002467>
23. C. Dorrer, N. Belabas, J.-P. Likforman, and M. Joffre, "Spectral resolution and sampling issues in Fourier-transform spectral interferometry," *JOSA B* 17, 1795-1802 (2000). DOI: <https://doi.org/10.1364/JOSAB.17.001795>
24. E. Khazanov, A. Shaykin, I. Kostyukov, V. Ginzburg, I. Mukhin, I. Yakovlev, A. Soloviev, I. Kuznetsov, S. Mironov, A. Korzhimanov, D. Bulanov, I. Shaikin, A. Kochetkov, A. Kuzmin, M. Martyanov, V. Lozhkarev, M. Starodubtsev, A. Litvak, and A. Sergeev, "eXawatt Center for Extreme Light Studies," *High Power Laser Science and Engineering* 11, e78 (2023). DOI: <https://doi.org/10.1017/hpl.2023.69>
25. Y. Peng, Y. Xu, L. Yu, X. WANG, Y. LI, X. LU, C. WANG, J. LIU, C. ZHAO, and Y. LIU, "Overview and status of station of extreme light toward 100 PW," *The Review of Laser Engineering* 49, 93 (2021). DOI: https://doi.org/10.2184/lsej.49.2_93
26. V. E. Leshchenko, "Coherent combining efficiency in tiled and filled aperture approaches," *Optics Express* 23, 15944-15970 (2015). DOI: <https://doi.org/10.1364/OE.23.015944>
27. L. Zhang, J. Chen, C. Ma, W. Li, Z. Qi, and N. Xue, "Research progress on on-chip Fourier transform spectrometer," *Laser & Photonics Reviews* 15, 2100016 (2021). DOI: <https://doi.org/10.1002/lpor.202100016>
28. R. Cheng, C.-L. Zou, X. Guo, S. Wang, X. Han, and H. X. Tang, "Broadband on-chip single-photon spectrometer," *Nature Communications* 10, 4104 (2019). DOI: <https://doi.org/10.1038/s41467-019-12149-x>